 doi:10.20944/preprints202211.0137.v1

Article

Elucidating the Role of Santalol as A Potent Inhibitor of Tyrosinase: *In Vitro* and *In Silico* Approaches

Nabeel Ali[1], Zainy Zehra[1], Anas Shamsi[1], Mohd. Amjad Beg[1], Zahoor Ahmad Parray[1], Israil[1], Md. Ali Imam[1], Naseem A Gaur[2], Md. Imtaiyaz Hassan[1], Anis Ahmad Chaudhary[3], Hassan Ahmad Rudayni[3], Mohammed Ibrahim Alghonaim[3] Sulaiman A. Alsalamah[3] and Asimul Islam*[1]

[1]Centre for Interdisciplinary Research in Basic Sciences, Jamia Millia Islamia, New Delhi-110025.
[2]International Centre for Genetic Engineering and Biotechnology, Aruna Asaf Ali Marg, New Delhi-110067, India.
[3]Department of Biology, College of Science, Imam Mohammad Ibn Saud Islamic University (IMSIU), Riyadh-11623, Saudi Arabia.
* Correspondence: **Author: Dr. Asimul Islam,** Associate Professor, Centre for Interdisciplinary Research in Basic Sciences, Jamia Millia Islamia, Email:aislam@jmi.ac.in, Mobile No: 00919312812007

ABSTRACT: This research work focuses on the potential application of an organic compound, santalol obtained from santalum album in the inhibition of the enzyme tyrosinase which is actively involved in the biosynthesis of the melanin pigment. Over-production of melanin causes undesirable pigmentation in humans as well as other organisms that significantly downgrade their aesthetic value. The study is designed to explain the purification of tyrosinase from the mushroom *Agaricus bisporus*, followed by activity assay and enzyme kinetic to give insight into the santalol modulated tyrosinase inhibition in a dose dependent manner. The multi-spectroscopic techniques like UV-vis, fluorescence, and isothermal calorimetry are employed to deduce the efficiency of santalol as potential candidate against the tyrosinase enzyme activity. Experimental results are further verified by molecular docking. Santalol derived from the essential oils of santalum album, is widely used as remedy for skin disorders and potion for fair complexion since ancient times. Based on enzyme kinetics and biophysical characterization, this is the first scientific evidence where santalol inhibits tyrosinase, which may be employed in agriculture, food, and cosmetic industries by prevent excess melanin formation or browning.

Keywords: Mushroom tyrosinase; Melanogenesis; Tyrosinase inhibitor; Multi-spectroscopic techniques; Natural compounds; tyrosinase inhibitor

1. INTRODUCTION

Melanin is a light-absorbing bio pigment, with coloration ranging from dark blackish-brown eumelanin to reddish-yellow pheomelanin [1]. This molecule imparts specific colorway to the skin, eyes, and hair in humans [2]. Melanin is also synthesized in various fruits and vegetables, which can be seen as a colored pigment. Melanin shields the skin from ultraviolet (UV) rays in the sunlight by absorbing the harmful radiation [3]. Thus, melanin production is an important process; contrariwise, there are occurrences where enhanced melanin production is a serious problem [4]. The skin disorders such as freckles, lentigo, melasma, or pigmented acne seen across all races are the result of an uncontrollable accumulation of melanin [5, 6]. These skin disorders not only affect the individual's physical appearance, but they may elicit social and mental insecurities resulting in lower quality of life (QOL) [7, 8]. Another grave concern is the process of neuromelanin occurring in the brain where dopamine is oxidized to dopaquinones by the action of tyrosinase [9]. Previous studies revealed that hyper tyrosinase activity in dopamine-rich nigral neurons can lead to neuronal tissue damage and apoptotic cell death. Neuromelanin is often associated with neurodegenerative diseases like Parkinson's disease and Huntington's disease [10]. Similarly, prolonged melanin synthesis develops brownish- black melanin

 doi:10.20944/preprints202211.0137.v1

spots over food stock such as fruits and vegetables subsequently leads to significant drop in their nutritional as well as market values accounting huge economical loss [11]. This biosynthetic reaction of melanin synthesis takes place in melanocytes where amino acid L- tyrosine is converted to end-product melanin in a series of steps with the participation of a key enzyme called tyrosinase [12, 13]. This enzyme catalyses two fundamental steps of melanin production which begin with the hydroxylation of monophenols to *o*-diphenols namely L-DOPA (L-3,4-dihydorxyphenylalanine) displaying its monophenolase activity. The second step is the oxidation of *o*-diphenols to *o*-quinones namely dopaquinone, presenting its diphenolase activity. Subsequently, *o*-quinones polymerize to produce melanin in a cascade of reactions [14] (**Fig. 1**). Evidently, tyrosinase is a polyphenoloxidase (EC 1.14.18.1), regulatory metallo-enzyme having two copper ions at its active site, with several isoforms. The enzyme is reported to have approximately 120 kDa of molecular mass, distributed among two H subunits each of ~43 kDa and two L subunits each of ~14 kDa, which is most common form of tyrosinase. Thus, exist as a H_2L_2 tetramer in holoenzyme state [15, 16]. It possesses two binding sites for the phenolic substrates along with a copper conjugated oxygen binding site. The fact that mushroom tyrosinase obtained from *Agaricus bisporus* have striking homology with mammalian tyrosinase [17], therefore makes it a convenient target for inhibition studies for therapeutics applications in human as well as in food industries as food preservatives [18].

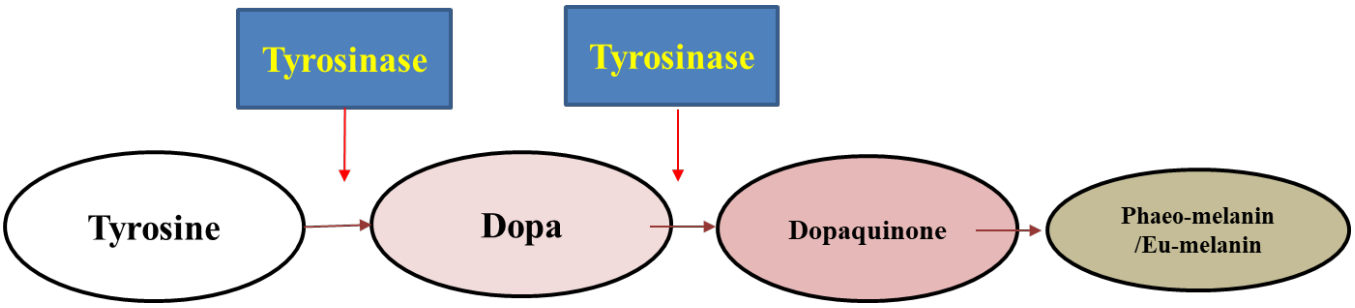

.

Figure 1. Conversion of tyrosine into melanin in presence of tyrosinase enzyme (tyrosine to melanin conversion pathway).

As stated above, tyrosinase acts as a rate-limiting enzyme in the melanin biosynthesis pathway. Thus, the primary approach to slow down the pathway is to inhibit tyrosinase via different strategies. Out of which, anti-tyrosinase action by chemical modalities such as kojic acid, arbutin and hydroquinones has been widely used. Although these compounds with both natural and synthetic origins have been reported to possess tyrosinase inhibitory properties, they are often limitation subject to their toxicity, activity, or stability [19-21]. Thus, a naturally occurring compound with an inhibitory effect on melanogenesis, serves as a good choice for commercial applications because of their organic nature, accompanied by less toxicity and highest compatibility when compared to their synthetic counterparts [22]. Therefore, we screened a phytochemical called Santalol, derived from the essential oils of sandalwood (*santalum album*). In traditional medicinal systems, it is widely used as a remedy for skin disorders and potion for fair complexion [23]. Chemically, santalol is a phenolic compound with good antioxidant abilities [24]. Also, it is approved by FDA for human use and consumption [25, 26]. Apparently, there is a lack of information on the pharmacological potency of santalol against tyrosinase activity [27]. Here, in this study, we have investigated its role as a tyrosinase inhibitor along with a plausible mechanism of inhibition by biophysical study. Furthermore, using multi spectroscopic techniques, we have elucidated the interaction mechanism of pure santalol compound towards purified enzyme tyrosinase, later confirmed by molecular docking results.

2. MATERIALS AND METHODS

2.1. Materials

 doi:10.20944/preprints202211.0137.v1

The target enzyme, tyrosinase was obtained from the edible mushroom (*Agaricus bisporus*). The test compound, Santalol (CAS no. 77-42-9) 80.9 % pure, dimethyl-sulfoxide (DMSO), 3, 4-Dihydroxyphenylalanine (L-DOPA), were bought from Sigma-Aldrich. All other reagents like phosphate buffer, Tris buffer, sodium chloride, SDS etc. of analytical grades were purchased from Merck ltd.

2.2. Methods

2.2.1. Extraction of the enzyme tyrosinase

The protocol of Haghbeen et. al., with few alterations, was carried out for extraction of mushroom tyrosinase [28]. The mushrooms tissues were made into a paste by a blender. The mushroom slurry so obtained was mixed with pre-prepared 200 mL of cold 50 mM phosphate buffer (pH 6.8) using 180-200 g of mushroom cap proportion. To get rid of various undesirable cellular products like cellulose and cell debris, centrifugation of homogenate for 30 min at 4200 g was performed to collect supernatant to be used as a source of enzyme. The pellet obtained after centrifugation was again mixed with cold phosphate buffer, left undisturbed on ice with intermittent shaking followed by another round of centrifugation to yield more enzyme from the supernatant.

2.2.2. Ammonium sulphate precipitation with dialysis

Ammonium sulphate precipitation was done by weighing the finely grounded ammonium sulphate and then mixed in the extract and keep stirring. The mix was centrifuged at 8000 g for 20 min at 4 °C. Different degrees of precipitation were tried for enzyme tyrosinase enzyme i.e., 30%, 60%, 90% and different precipitates were collected. Dialysis was conducted for different precipitates against 50 mM potassium phosphate buffer (pH 6.8) continuously for 24 h and the buffer was changed periodically after every 7-8 hours [29]. The fraction of protein obtained after last dialysis was chosen for the study [30, 31].

2.2.3. Purification of enzyme tyrosinase using chromatography

The purification of crude enzyme obtained after dialysis, was exposed to a couple of chromatographic techniques viz. ion-exchange chromatography and gel filtration to get the protein sample in its highest purity. Firstly, crude protein extract was subject to ion-exchange chromatography using the DEAE-Cellulose column (20 × 1 cm). The prepared sample having approximately 3 ml of aqueous protein (using 3ml loop) was poured into the DEAE-cellulose column. The column was first pre-equilibrated with potassium phosphate buffer (50 mM, pH 6.8, and then washed with equilibration buffer. The protein elutions were designed in the linear gradient of 0–500 mM NaCl and 0–100 mM potassium phosphate buffer keeping the 0.5 mL per min flow rate. The eluted fraction of protein obtained from the ion-exchange column was then applied to *Superdex 200 pg* column for gel filtration. The column was pre-equilibrated with a 50 mM phosphate buffer of pH 6.8. The protein was eluted in the equilibration buffer at a flow rate of 0.5 mL/min. The samples collection was done at 4 degrees Celsius. The active fractions were pooled, dialyzed against the 50 mM phosphate buffer of pH 6.80, and concentrated [32]. The fractions (3 mL each) were collected for SDS-PAGE. An SDS-PAGE of 12% separating gel and 4% stacking gel was prepared by the method of Laemmli, 1970 [33]. The previously pooled samples were prepared by adding 1% (w/v) SDS and then boiling for 5 min at 100°C in eppendorfs. To visualize the purified protein, gel electrophoresis was run in Tris-HCl buffer of pH 8.4 at 80-100 V for 3 hr. After electrophoresis, the protein bands on the gel were made detectable by staining with standard Coomassie Brilliant Blue. Samples showing the discrete band in SDS-PAGE were assayed for tyrosinase activity [32, 34].

2.2.4. Tyrosinase activity assay

The enzyme activity of tyrosinase was assessed by performing absorption spectroscopy where the rate of conversion of L-DOPA (substrate) to dopachrome (a red-coloured

Preprints (www.preprints.org) | NOT PEER-REVIEWED | Posted: 8 November 2022 doi:10.20944/preprints202211.0137.v1

oxidised product) was monitored. An aliquot containing purified tyrosinase enzyme was incubated for 5 min at 298 K, L-DOPA solution (4 mg/mL) as substrate was added to the reaction mixture for measurement at 473 nm. After incubation for additional 5 min, the mixture was shaken again, and a second reading was measured for 10 minutes. The change in absorbance appeared to be proportional to enzyme concentration [35]. Zymography was also performed in order to measure the enzymatic activity of the purified enzyme. Similar Protocol was followed as explained by Wilkesman et al.[36].

2.2.5. Tyrosinase inhibition kinetics and UV-visible spectral measurements

The anti-tyrosinase activity of santalol was measured using UV–Vis spectroscopy. Absorption measurements were carried out using a Jasco F-660 UV spectrometer in a 1.0 cm quartz cuvette at room temperature. The change in absorbance at 473 nm was measured, by subsequently adding santalol but keeping protein concentration constant in each reading as described in various reports [37, 38]. We also have monitored overall spectral changes before and after addition of santalol in the purified tyrosinase enzyme at pH 6.8. Before every measurement all the samples were incubated for 5-10 min at RT and the spectra were measured in the range of 240-340 nm [39].

2.2.6. Intrinsic fluorescence binding study

The binding affinity of santalol towards purified protein tyrosinase was evaluated by examining changes in the fluorescent intensities [40, 41]. These quenching experiments were performed on a spectrofluorometer (Model no. FP-6200). Slit widths of 10 nm, quartz cuvette with 1 cm path length was used for both emission and excitation, and temperatures were set to 298 K. Measurements were performed with 25 μM tyrosinase in 30 mM potassium phosphate buffer of pH 6.8, with excitation wavelength set at 280 nm and emission spectra recorded between 300- 400 nm. Mathematical evaluation of fluorescence quenching data was done using stern-Volmer and modified Stern-Volmer plot [40].

2.2.7. Isothermal titration calorimetry (ITC)

To evaluate the thermodynamic parameters and binding interaction of tyrosinase with ligand molecules in the buffer solution, ITC was used. The isothermal titration calorimetry (ITC) is the excellent method to elucidate binding interaction and for that VP-ITC Calorimeter (MicroCal, 22 Industrial Drive East, Northampton, MA 01060, United States) apparatus was utilized. The experiments were carried out at 25 °C at pH 6.8 using 25 mM phosphate buffer, the calorimeter cell was injected with a 30 μM of the protein solution (tyrosinase). The ligand (santalol) of 900 μM was titrated in the cell, each ligand solution was loaded with 10-microliter aliquots in each 260-second step through the syringe. The data was normalized against the results of titration of santalol into tyrosinase and was evaluated by the MicroCal Origin ITC software, by three-step sequential binding model as reported earlier [42-44] which could fit to the data to generate the change in binding enthalpy (ΔH^o), change in entropy (ΔS^o) and the association constant (K_a). By these primary measurements, secondary parameter change in Gibbs free energy (ΔG^o) can be calculated by using the relation:

$$\Delta G^\circ = -RT \ln K_a = \Delta H - T\Delta S \qquad (1)$$

where R is the gas constant and T is the absolute temperature.

The heat of dilution of the ligand in phosphate buffer was subtracted from the titration data. MicroCal Origin 8.0 was used to calculate the stoichiometry of association constant (K_a), enthalpy change (ΔH), and binding (n).

 doi:10.20944/preprints202211.0137.v1

2.2.8. Molecular docking analysis

To get more comprehensive information about the inhibitory mechanism between santalol and tyrosinase, molecular docking studies were performed by using Autodock 4.0. The three-dimensional (3D) crystal structure of *Agaricus bisporus* tyrosinase (PPO3) was obtained from RCSB PDB databank PDB ID: 2Y9X (https://www.rcsb.org/structure/2Y9X/_ [21598903]. InstaDock [45] was used in molecular docking learning approach which prepare the receptor molecule pdb format into pdbqt at the push of a simple click [33105480; 34293449]. PPO3 (tyrosinase) includes two copper atoms that participate directly involved in the numerous catalytic activities. The target ligands were docked on a predefined catalytic site so using PyMOL and AutoDock Vina to determine the 3D grids of the target protein PPO3 [30521996; 19499576; 34469971]. The compound's structure was derived from PubChem database (https://pubchem.ncbi.nlm.nih.gov/) in SDF format for ligand preparation, where the energy minimization and PDBQT file convert was done via PyRx 0.8 [25618350]. Assortment of the binding affinities scores, further switch on the studies of the receptor-ligand interaction which interprets the interacted residues into the catalytic sites. The conceivable dock conformations of the 2D ligand-receptor interactions by using Discovery Studio [20401516; 33592201]. Further, binding analysis by using the visualization approach was carried out to understand the binding pattern of the ligands with a receptor. Then the further evaluation was carried out based on interactions to avoid false positives and select highly interactive with binding pocket of PPO3.

3. RESULTS AND DISCUSSION

3.1. Extraction of enzyme tyrosinase and ammonium sulphate precipitation

A cell-free mushroom tyrosinase system was used to conveniently extract the target protein. A total of 310 ml crude protein extract was used from the 200 grams of mushroom taken as the source. The ammonium sulphate precipitation method is used to precipitate the crude protein by saturating the crude solution with finely divided ammonium sulphate in a stepwise manner. The concept of salting-out was applied where higher salt concentrations decrease the protein solubility in a solution leading to precipitation of protein which eventually comes out of the solution and can easily be recovered after centrifugation [46, 47] we have obtained most of the protein including the target protein (protein of interest, tyrosinase) in 60 % fraction of ammonium sulphate salt concentration.

3.2. Purification of enzyme tyrosinase using chromatography

The target protein is often accompanied by other proteins and organic molecules which tend to accumulate during homogenized extract preparation. The two-step purification was performed to segregate target protein from the mixture using ion-exchange and gel filtration chromatography. When dialyzed protein sample was applied to a DEAE-Cellulose column with stepwise increment in NaCl gradient, the target protein was eluted at 0–100 mM NaCl with phosphate buffer of same 6.8 pH. (The result is illustrated in supplementary Fig. S1). DEAE is basically positively charged resin that binds to, or exchanges opposite charged (negatively charged) protein molecules present in protein mixture at particular operating pH. The eluted active fractions having maximum absorbance at 280 nm were mixed, concentrated, and then loaded to *Superdex 200 pg* gel filtration column in order to obtain the purest form of tyrosinase [48, 49].

Preprints (www.preprints.org) | NOT PEER-REVIEWED | Posted: 8 November 2022 doi:10.20944/preprints202211.0137.v1

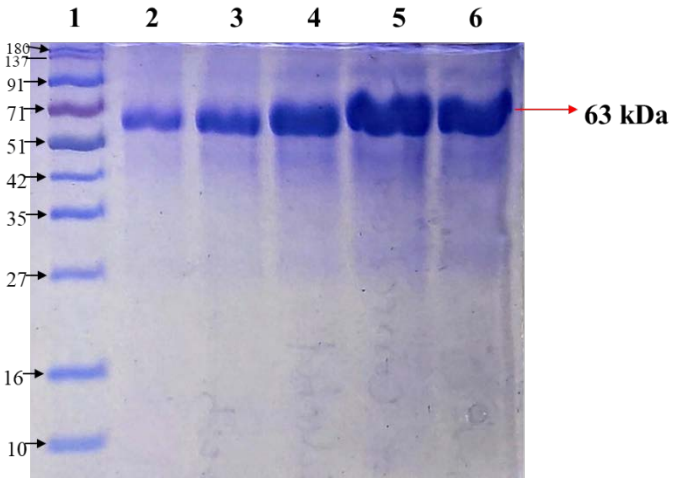

Figure 2. SDS-PAGE profile indicating 63 kDa purified form of tyrosinase, lane 1 showing protein marker and lane 2-6 depicts the purified tyrosinase loaded in gradient (lane 5, 6 represent highest conc. of protein).

Each of the peaks obtained after ion-exchange chromatography was collected as separate aliquot and run on SDS-PAGE. The purified protein obtained after both chromatographic techniques showed a single band of 63 kDa as shown in **Fig. 2**. The final eluted fraction showed major peaks of tyrosinase activity which were observed in active fractions with a final specific activity. SDS-PAGE of the enzyme after two step-purification showed that the resolved electrophoretic bands were progressively improved from the crude extract to the final step of the gel filtration column chromatography. It revealed only a single distinctive protein band for the pure form of tyrosinase with an apparent molecular weight of 63 kDa obtained. Total amount and concentration of protein so obtained after every step of purification was estimated with BSA as a standard and percentage yield is summarised in **Table 1**.

Table 1. Purification summary of tyrosinase.

S. No.	Purification Steps	Fraction Volume (ml)	Protein conc. (mg/ml)[b]	Total amt. of protein (mg)	Total Activity (units)	Specific activity (Unit/mg)	Yields (%)	Purification Fold
1	**Crude extract** [a]	310.0	1.250	387.5	4121	10.6	100	1
2	**Ammonium sulphate precipitation 30% cut-off**	120	0.853	102.36	3172	30.9	26.42	2.91
3	**Ion- exchange chromatography, DEAE-Sepharose column**	65	0.552	35.88	2627.5	73.25	9.25	7.07
4	**Gel filtration chromatography, using Superdex 200 column**	45	0.15	7	2256.2	322.3	1.8	32.14

[a] from 200 g of wet weight of mushroom cap edible portion.
[b] Protein concentration determined by Bradford assay [55] using BSA as a standard protein.

3.3. Tyrosinase activity assay

Preprints (www.preprints.org) | NOT PEER-REVIEWED | Posted: 8 November 2022 doi:10.20944/preprints202211.0137.v1

UV-vis absorbance spectral analysis is a widely used methodology to explore the conformational changes occurring in the protein with respect to the formation of protein-ligand complexes. The purified protein so obtained after two-step purification, was first subjected to its activity determination using UV-visible spectroscopy and Zymogram analysis. The initial rate of reaction is proportional to the concentration of the enzyme. One unit of enzyme corresponded to the amount which catalysed the transformation of 1 µmol of substrate to product per min under the above conditions and produced changes in absorbance. It has been observed that dopachrome gives maximum absorption at 473 nm [39]. Therefore, we monitored the change in absorption till horizontal line or point of saturation of the enzyme was achieved, in other words, purified tyrosinase activity was monitored till no L-DOPA (substrate) remains for the enzyme to be converted into the product (dopachrome). As tyrosinase protein activity is based upon the change of color of L-DOPA substrate to red pigment dopachrome **(Fig. 3).** The intensity of colour is directly proportional to tyrosinase concentration. Zymogram obtained after native -PAGE of purified protein is depicted in **Fig. 3** below. Formation of melanin was also confirmed by incubating the native PAGE for zymography for about 24 hours (Supplementary Fig. S3).

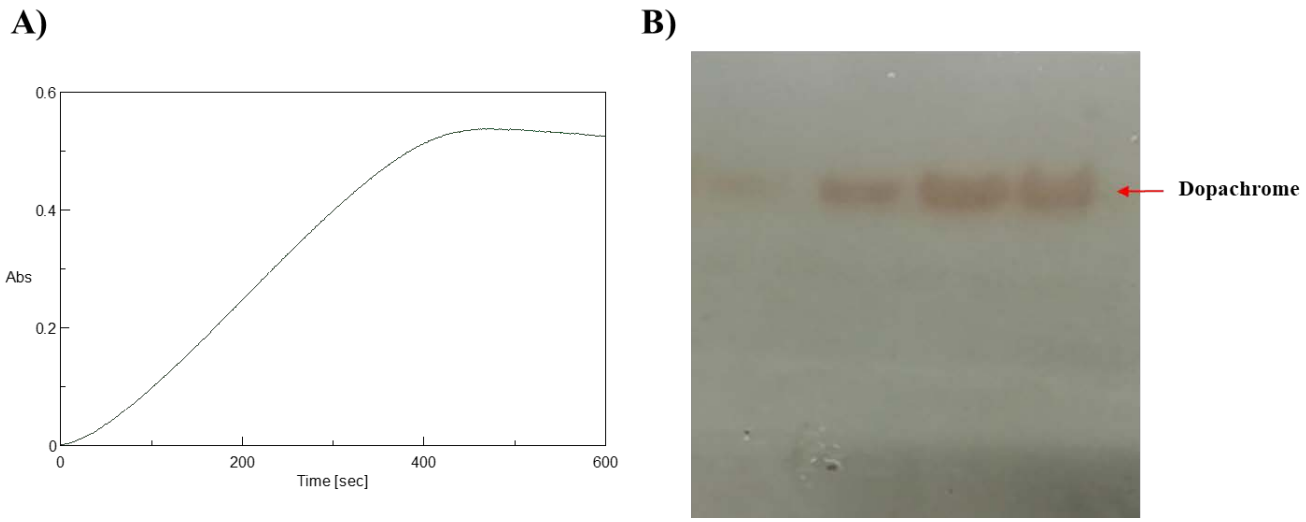

Figure 3. A) Change in absorbance was monitored at 473 nm (dopachrome λ_{max} = 473). **B)** Dopachrome was formed upon addition of tyrosine as substrate in an enzyme mixture proven the active form of tyrosinase in reaction mixture. Native-PAGE gel was incubated in 5 mM L-tyrosine (substrate) at 37 degree, bands of light red coloured pigment dopachrome (shown right side) was appeared after few minutes of incubation which eventually leads to production of melanin dark brown color (shown in fig. 3 right side).

3.4. Tyrosinase inhibition kinetics

Changes in tertiary structure of tyrosinase was monitored using far UV-visible scan 340-240 nm. We observed with increase in santalol concentration from 0 µM to 50 µM, there was perturbation in tertiary structure of tyrosinase, which was later confirmed by plotting absorption maxima at 280 nm ($A_{280\ nm}$) vs santalol concentration (**Fig. 4A**) To elucidate the activity of tyrosinase obtained after purification, enzyme kinetics study was performed in absence as well as in presence of santalol as tyrosinase inhibitor. Linearised data obtained from change in absorbance per unit time, was fitted in Michaelis-menten equation using GraphPad prism and sigma plot software version 12.5. The enzyme kinetics as measured by the Michaelis constant (K_m), is defined as the substrate concentration at which half of the maximum velocity or the rate of enzymatic reactions achieved. The Michaelis-menten constant (K_m) value of the purified tyrosinase was estimated in a given range of substrate concentrations, L-Dopa (Supplementary Figure S2). In order to calculate exact K_m values with different concentrations of inhibitor Lineweaver-Burk plot was drawn. The apparent K_m value of protein was calculated from the Lineweaver-Burk plots

Preprints (www.preprints.org) | NOT PEER-REVIEWED | Posted: 8 November 2022 doi:10.20944/preprints202211.0137.v1

relating 1/V to 1/[S]. We observed overall decrease in enzyme activity of tyrosinase with increase in concentration of santalol as inhibitor. Maximal inhibition was found to be around 50 µM of santalol.

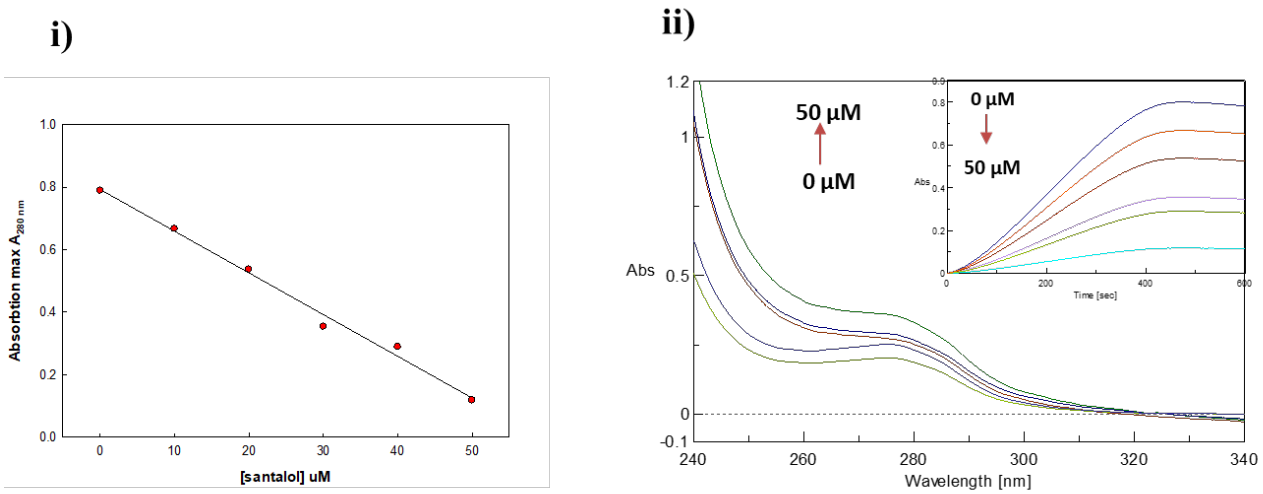

Figure 4. A) i) Effect of various concentration of compound santalol as tyrosinase inhibitor on Absorbance maxima $A_{280\ nm}$ values, ii) Effects of varying concentrations of santalol on tyrosinase tertiary structures monitors using far UV-visible spectroscopic scan, inset figure showing progressive tyrosinase inhibition with increase in santalol concentration (µMolml^{-1}).

Using the linearised data obtained by Michaelis-Menten plot, the inhibitory type was also determined by the Lineweaver-Burk plot (**Fig. 4B**), for simplicity four major concentrations was shown in plot. Plots clearly shown decrease in overall activity of purified tyrosinase with increase in santalol concentration (in dose-dependent manner). Santalol might get bind to the active site of tyrosinase in competitive manner such a way that its substrate (L-dopa, used in this study) is no more accessible to the enzyme for binding, thus its final product eumelanin or dopachrome not formed. On the basis of calorimetric assay also the inhibition of tyrosinase by santalol was confirmed using UV-visible spectroscopic measurement at 473 nm (Figure S4).

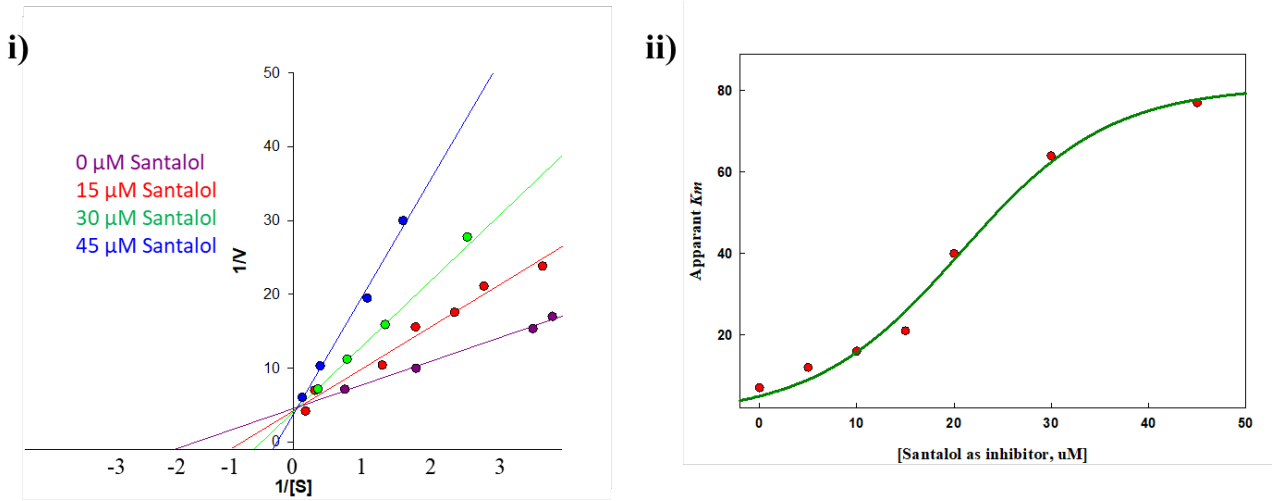

Figure 4. B: i) Lineweaver-Burk plot in presence of various concentration of santalol, right-hand side (figure ii) depicts increase in K_m values were also observed in dose-dependent manner.

Preprints (www.preprints.org) | NOT PEER-REVIEWED | Posted: 8 November 2022 doi:10.20944/preprints202211.0137.v1

3.5. Intrinsic fluorescence binding study

Intrinsic fluorescence study is carried out to examine interactions between protein and the ligand. This can clue us various parameters for drug-protein binding. The intrinsic protein fluorescence is mainly due to aromatic residues like tyrosine, tryptophan, and phenylalanine in the protein sequence where they act as a sensitive fluorescent probes to investigate protein interactions with particular ligand. In addition, strong binding affinities exists between santalol and tyrosinase possibly due to the presence of hydroxyl group in santalol. From the result of the intrinsic fluorescence spectra, we observed that santalol binding to the tyrosinase lead to conformational changes in tyrosinase that result in gradually decrease in the spectra in a dose-dependent manner **(Fig. 5A).** Although the decrease in the fluorescence intensities were caused by quenching, there was no significant wavelength shift indicating that tyrosinase does not undergo unfolding or denaturation after binding with the compound santalol.

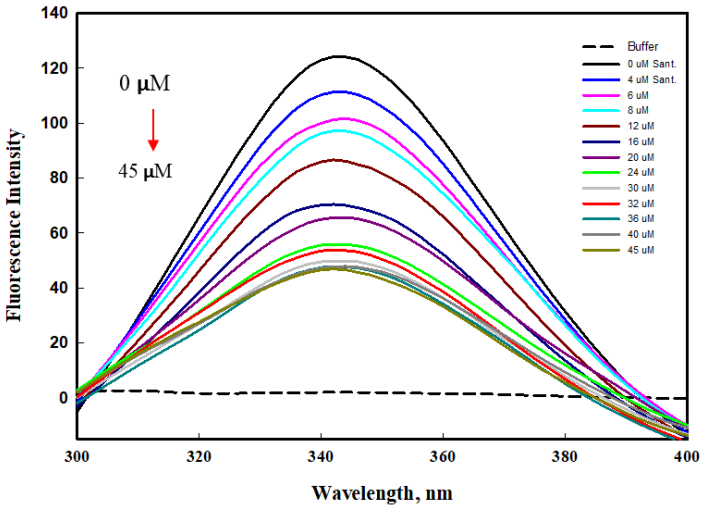

Figure 5. (A): Intrinsic fluorescence spectra of tyrosinase in the presence santalol at various concentrations, which were ranges from 0- 40 µM for top to bottom curves, respectively.

To identify the interaction mechanism of ligand santalol with enzyme tyrosinase, the data of fluorescence quenching were presented in the form of a Stern-Volmer plot, using the following equation:

Fluorescence quenching was described by the Stern-Volmer equation.

$$\frac{F_0}{F} = 1 + K_{SV}\,[C] \qquad (2)$$

where, F_0 = fluorescence intensities before the addition of the quencher; F= fluorescence intensities after the addition of the quencher; k_q = Bimolecular quenching constant τ0 = Lifetime of the fluorophore in the absence of the quencher; [Q] = Concentration of the quencher, and K_{SV} = Stern-Volmer quenching constant.

The value of K_{sv} determined by the linear regression plot of F_0/F vs. [Q] at 298 was 5.32×10^4. The plot in the Fig 5B. showed a good linear relationship, indicating that a single type of quenching process (static or dynamic quenching) occurred during the formation of santalol-tyrosinase complex. For static quenching interactions, if there are similar and independent sites in biological molecules, the apparent binding constants (K_a) and the number of binding sites (n) can be obtained from the following equation:

$$\log (F_0 - F)/F = \log K_a + n\log Q1/2 \qquad (3)$$

Preprints (www.preprints.org) | NOT PEER-REVIEWED | Posted: 8 November 2022 doi:10.20944/preprints202211.0137.v1

According to the intercept and slope value of the regression curve **(Fig. 5B),** the values of K_a and n for ligand–tyrosinase interaction were calculated based on equation (3). The K_a value of 1.64 x 10^5 L/mol achieved the order of magnitude of 10^5 L/mol, indicating the strong binding of ligand to binding pocket of enzyme tyrosinase. Also, the value of *n* was close to one, suggesting that there was a single binding site or a single class of binding sites in tyrosinase for the given ligand.

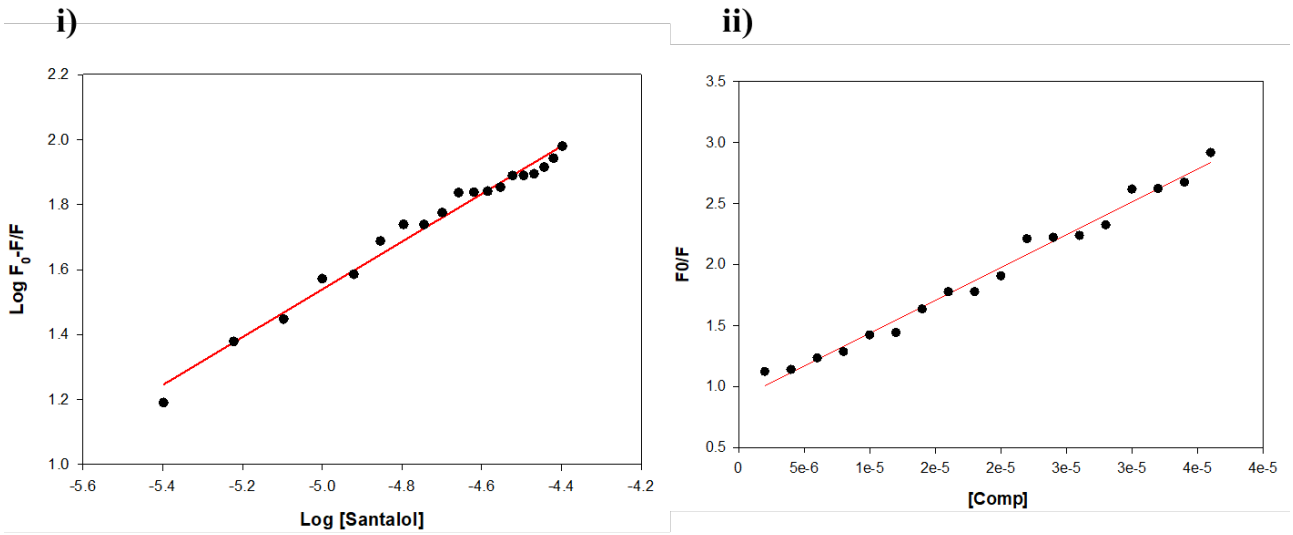

Figure 5. (B): Stern– Volmer and modified Stern-Volmer plots for the fluorescence quenching of tyrosinase at 298K by santalol.

3.6. Isothermal titration calorimetry (ITC)

Isothermal titration calorimetry (ITC) measurements were taken to know the binding affinity of santalol with the purified tyrosinase. ITC is the widely used technique to deduce the interactions between proteins and other molecules based on change in energy when the two moieties or molecules binds to one another. **Fig. 6** depicts graphical outcomes of titrated santalol (ligand) with the protein, tyrosinase. The top-panel in the figure gives the raw data in power versus time (heat per unit of time liberated from every injection of the ligand with respect to the protein) while the lower panel in the figure displays the raw data in power standardized to the amount of the injectant (kcal mol^{-1}) versus its molar ratio of santalol injections into the cell containing tyrosinase. From the data the thermodynamic binding parameters were calculated can be seen in which showed change in enthalpy (ΔH^o), the association constant (K_a), and the equilibrium dissociation constant and change in free energy (ΔG^o) which was estimated using equation given below. From **table 2** it can be observed that ΔG^o is negative signifies bi-molecular reaction is spontaneous and negative enthalpy change signifies the process is exothermic in nature.

Preprints (www.preprints.org) | NOT PEER-REVIEWED | Posted: 8 November 2022 doi:10.20944/preprints202211.0137.v1

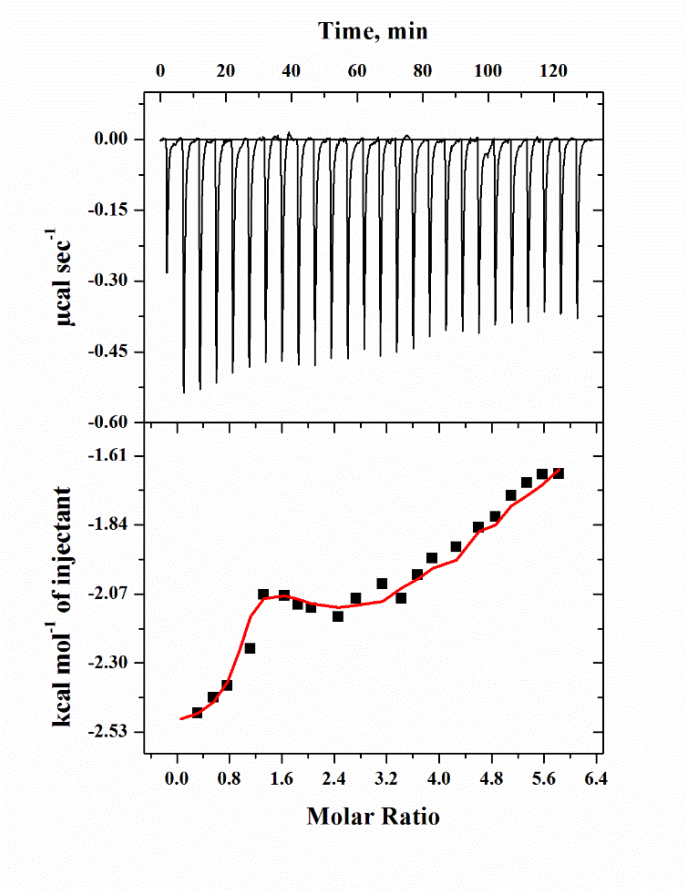

Figure 6. Isothermal titration calorimetry (ITC) profile of tyrosinase-santalol binding: Calorimetric responses owing to consecutive injections of santalol in the ample cell with tyrosinase are depicted in upper section whilst the lower section depicts integrated heats of interactions as the function of the [santalol]/ [Tyrosinase] molar ration.

Table 2. Calorimetric binding parameters obtained by analysis of ITC measurements on interaction of santalol with purified tyrosinase at 298 K (25 °C) and pH 6.8.

Thermodynamic parameters (Units)	Step1	Step2	Step 3
K_a (M^{-1})	$7.89 \times 10^5 \pm 8.5 \times 10^4$	$1.32 \times 10^4 \pm 1.7 \times 10^3$	$2.49 \times 10^3 \pm 2.8 \times 10^2$
ΔH^o (cal mol^{-1})	-2.595×10^3	-6.497×10^3	-4.16×10^4
ΔS^o (cal $mol^{-1}deg^{-1}$)	18.3	-2.94	-124
ΔG^o (cal mol^{-1})	$-8.048 \times 10^3 \pm 90.0$	$-5.62 \times 10^3 \pm 7.87 \times 10^2$	$4.16 \times 10^3 \pm 90.0$

3.7. Molecular docking analysis

The crystal structure of PPO3, a tyrosinase enzyme having two molecules which have tetramer chains. The first is polyphenol oxidase are tetramer A, B, C, D chains having 2-392 residues and second lectin-like fold protein are tetramer E, F, G, H chains having 9-150 residues. In order to acquire more in-depth information on the competitive inhibition

Preprints (www.preprints.org) | NOT PEER-REVIEWED | Posted: 8 November 2022 doi:10.20944/preprints202211.0137.v1

mechanism between Santalol and PPO3 (tyrosinase) and using Kojic acid as standard, molecular docking studies were performed by using InstaDock. In molecular docking, the compounds produced log files, where the affinity (kcal/mol) obtained and docked poses for discrete compounds analyzed. The experiential binding free energy for the Santalol-PPO3 tyrosinase complex was -5.802 kcal mol^{-1} (-24.283 k J mol^{-1}) and the standard Kojic acid complex was -5.408 mol^{-1} (-22.608 k J mol^{-1}). The binding free energy calculations shows that Santalol binds to PPO3 tyrosinase protein more firmly than Kojic acid and the detailed of energies calculation in mentioned in **Supplementary Fig. S5 & Table S1**. To discover the active sites of tyrosinase, look for neighbouring Cu atom residues that are involved in diverse catalytic activities are HIS61, HIS85, PHE90, HIS94, HIS259, HIS263, PHE292, HIS295 and HIS296 which are shown in **Fig. 7 (A-B)**. In previous studies, the cavity of tyrosinase comprises two sites: the peripheral and the active site therefore it could be seen in **Fig. 7 (B)** copper as presented in a yellow sphere which is in **Fig. 8 (B)** brown in color, docking studies determined the Cu B site has most conspicuous binding in comparison to Cu A which means it was more tightly bound to the hydroxyl group.

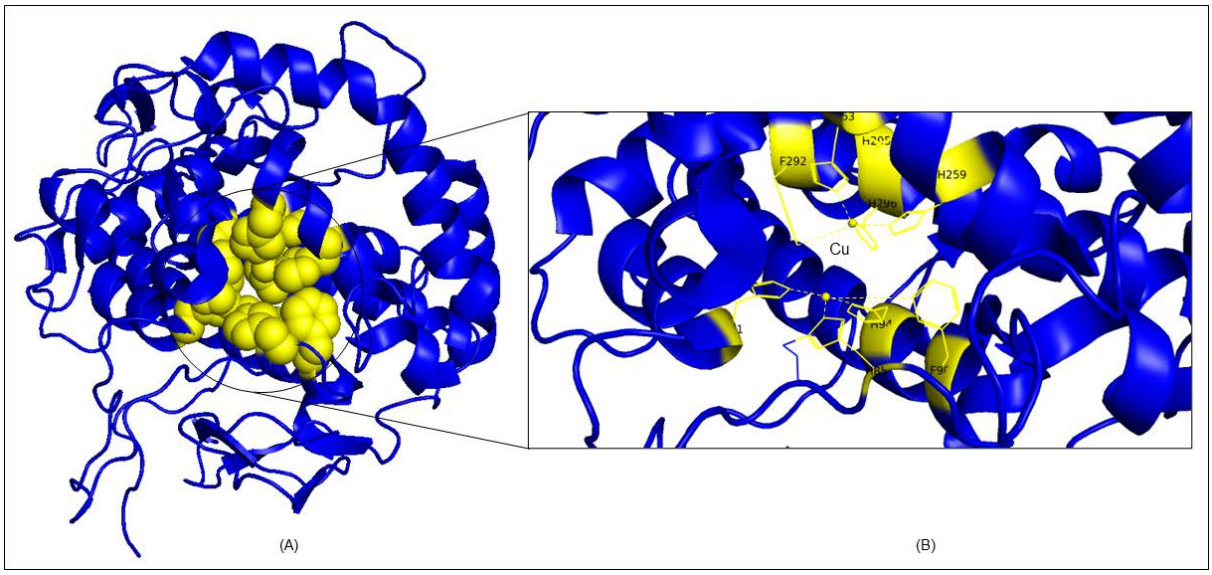

Figure 7. Ligand Binding pocket studies (A) Cartoon representation of PPO3 tyrosinase PDB ID: 2Y9X (blue) showing the catalytic sites in Sphere shape (yellow). B) Nearby Copper (Cu) atom residues are involved in various catalytic activities.

In molecular interaction studies of Santalol-PPO3 tyrosinase complex revealed it is closely bound to the true conformation active sites contains most likely on the catalytic sites which is shown in **Fig. 8 (A-C)**. As shown in **Fig. 8 (A)** the 3D surface representation of the Santalol-tyrosinase complex clearly shows the cavity of the binding pocket whereas in **Fig. 8 (B)** shows the cartoon representation of tyrosinase protein complex with Santalol and their interaction are clearly visible but in **Fig. 8 (C)** there is the 2D interaction diagram probed several interacting residues in expand form was HIS61, HIS244, VAL248, HIS259, ASN260, HIS263, PHE264, MET280, SER282, VAL283 and ALA286 were involved in hydrogen bonding and hydrophobic interactions. The hydroxyl group of Santalol was oriented towards copper (Cu) B and it was near to MET280 and SER282 which formed a hydrogen bond with 2.26 and 3.35 Å distance.

Preprints (www.preprints.org) | NOT PEER-REVIEWED | Posted: 8 November 2022 doi:10.20944/preprints202211.0137.v1

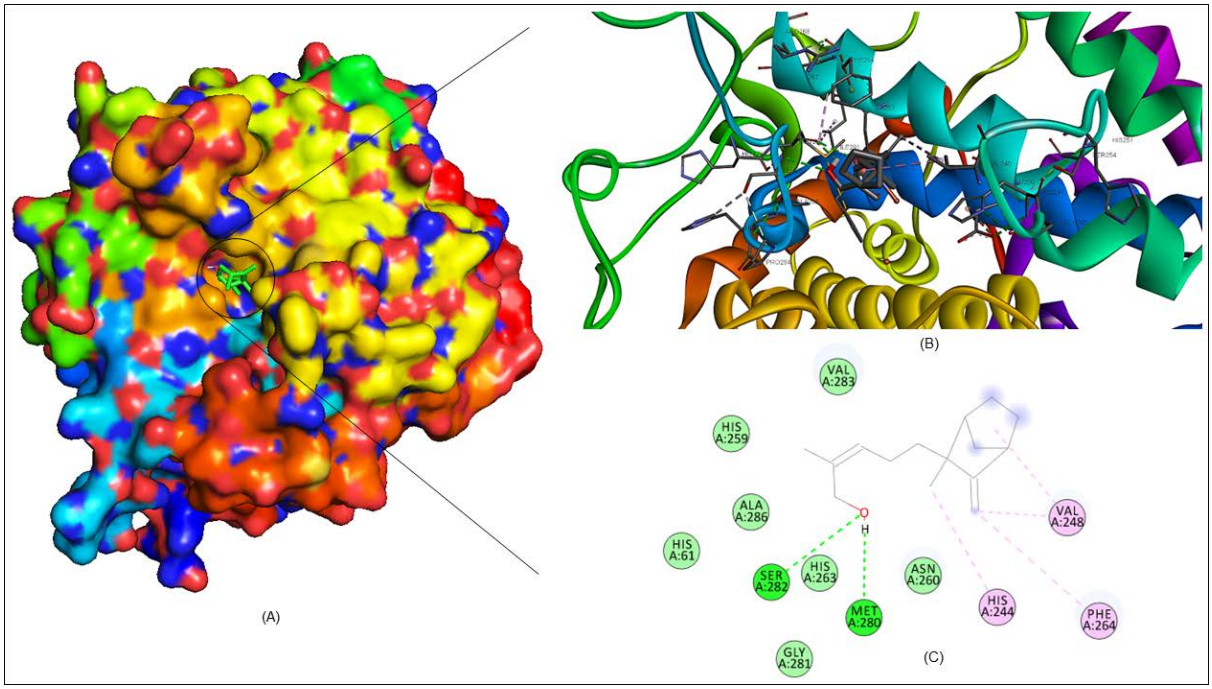

Figure 8. Molecular interaction studies showing the Santalol-PPO3 tyrosinase complex (A) the surface model of Santalol-PPO3 tyrosinase complex was in active pocket. (B) Cartoon representation of tyrosinase protein complex with Santalol showing the interacted residues in expand form (C) The 2D interaction analysis of complex files was done by BIOVIA here, and the different colour showing bonds are Light Green_Carbon hydrogen bond; Green_Hydrogen bond and Purple_Pi Alkyl bond.

As far as given label of santalol's "safe-to-use" is concerned [50], Toxicity evaluation of Santalol with machine learning methods using pkCSM server [51] were performed (supplementary Table S1and S2). All the predicted outcomes obtained fallen under the category of safe to use which correlate with origin of natural source i.e., sandalwood oil.

4. CONCLUSION

Tyrosinase is the major enzyme responsible for the synthesis of melanin pigment, but the hyper-pigmentation associated with the enhanced activity of tyrosinase is highly undesirable. It promotes unwanted food browning and dermatological disorders in human. Thus, screening and elucidation of the potential inhibitor for this enzyme serve good application in commercial domains such as agriculture, medicine, cosmetics industry, and other pharmacological sectors. Despite the presence of a wide array of reported tyrosinase inhibitors, very few of them are non-toxic and effective at the same time. In this study, we propose a *safe-to-use* phytochemical called santalol derived from sandalwood with anti- tyrosinase activity. A plausible kinetic mechanism analyzed by UV-visible spectroscopy is presented where santalol mediate competitive inhibition as it fits into the catalytic pocket of the enzyme and alters its structure which hinders the binding of the original substrate L-tyrosine. Furthermore, the fluorescence quenching study and isothermal titration calorimetry also suggested that there is a very strong binding between tyrosinase and the test compound, santalol, in accordance with the molecular docking study. Our results indicate that santalol may serve as a novel as well as natural anti-tyrosinase agent, although the clinical and industrial trials are yet to be elucidated. Santalol had been used since ancient time for beautification purposes, but detailed mechanism of action of inhibition is not unveiled therefore this is the first study which provides possible mechanism for santalol action on tyrosinase activity as well as effect of santalol compound on structural integrity. However, the findings we attained here in this study need further investigation in pigment cell assays or in animal models and in clinical studies.

Authors Contribution: Nabeel Ali: Conceptualization, writing-review and editing, Analysis of data, data Curation; **Zainy Zehra**: writing, Editing, Data curation; **Anas Shamsi:** data validation, Resources, Visualization, Writing-review and editing; **Naseem A. Gaur:** Writing-review and editing; **Md. Imtaiyaz Hassan:** Visualization, Data validation; **Israil:** Writing-review and editing; **Mohd. Amjad Beg & Md. Ali Imam**: Molecular Docking; **Zahoor Ahmed Parray:** Isothermal Titration calorimetry experiment and data analysis, Data validation, Investigation; **Anis Ahmad Chaudhary:** Resources, Visualization**; Hassan Ahmad Rudayni:** data Curation**; Mohammed Ibrahim Alghonaim:** Visualization**; Sulaiman A. Alsalamah:** data Curation; **Asimul Islam:** Methodology, Investigation, Data curation, Supervision, Visualization, Writing-review and editing, formal analysis, Project Administration, writing-original draft.

FUNDING AND ACKNOWLEDGMENTS: The authors extend their appreciation to the Deanship of Scientific Research at Imam Mohammad Ibn Saud Islamic University (IMSIU) for funding and supporting this work through Research Partnership Program no. RP-21-09-86.

CONFLICTS OF INTEREST: The authors declare that they have no known competing financial interests or personal relationships that could have appeared to influence the work reported in this paper.

DATA AVAILABILITY STATEMENT:

All data generated or analyzed during this study are included in this manuscript and supplementary materials attached to this article

Supporting Information: Figure S1 (A): Elution profile on DEAE-Cellulose column chromatography. A linear gradient of NaCl was 0–100 mM. **(B)** Gel filtration profile using Superdex 200 pg column showing large peak (peak I) of tyrosinase using concentration protein fraction obtained after Ion-exchange chromatography. **Figure S2:** Michaelis-menten kinetics in presence and absence of santalol as inhibitor (0-50 μM). **Figure S3:** native-PAGE Profile (zymogram) obtained after incubation in tyrosine substrate solution 5mM for about 24 hours indicating the formation of dark-brown melanin pigment (loaded in increasing concentration gradient from lane 1 to lane 5. **Figure S4:** Colorimetric assay done in presence and absence of Santalol & kojic acid. **Figure S5:** 2D ligand interaction studies in between (a) Kojic acid-tyrosinase and (b) Santalol-tyrosinase complex.

CONFLICT OF INTEREST:

The authors declare that they have no known competing financial interests or personal relationships that could have appeared to influence the work reported in this paper.

REFERENCES

1. Kamilah, S.N., et al. Phenotypic Variation in Pigmentation of Persons with Albinism in Rejang Lebong, Bengkulu. in 3rd KOBI Congress, International and National Conferences (KOBICINC 2020). 2021: Atlantis Press.
2. Battistella, C., et al., *Bioinspired chemoenzymatic route to artificial melanin for hair pigmentation.* Chemistry of Materials, 2020. **32**(21): p. 9201-9210.
3. Solano, F., Photoprotection and skin pigmentation: Melanin-related molecules and some other new agents obtained from natural sources. Molecules, 2020. **25**(7): p. 1537.
4. Azumi, J., et al., The organogermanium compound THGP suppresses melanin synthesis via complex formation with L-DOPA on mushroom tyrosinase and in B16 4A5 melanoma cells. International journal of molecular sciences, 2019. **20**(19): p. 4785.
5. Hexsel, D., et al., *Epidemiology of melasma in B razilian patients: a multicenter study.* International journal of dermatology, 2014. **53**(4): p. 440-444.
6. Suh, A., et al., Adipose-derived cellular and cell-derived regenerative therapies in dermatology and aesthetic rejuvenation. Ageing research reviews, 2019. **54**: p. 100933.
7. Hongbo, Y., et al., Translating the science of quality of life into practice: what do dermatology life quality index scores mean? Journal of Investigative Dermatology, 2005. **125**(4): p. 659-664.
8. Khalilzadeh Ganjalikhani, M., et al., Studying the effect of structured ostomy care training on quality of life and anxiety of patients with permanent ostomy. International wound journal, 2019. **16**(6): p. 1383-1390.
9. Wang, D., et al., Fluorometric atrazine assay based on the use of nitrogen-doped graphene quantum dots and on inhibition of the activity of tyrosinase. Microchimica Acta, 2019. **186**(8): p. 1-7.
10. Ogawa, T., et al., Role of neuroimaging on differentiation of Parkinson's disease and its related diseases. Yonago acta medica, 2018. **61**(3): p. 145-155.
11. Zhou, X., et al., Full inhibition of Whangkeumbae pear polyphenol oxidase enzymatic browning reaction by L-cysteine. Food chemistry, 2018. **266**: p. 1-8.

12. Chen, C.-Y., et al., An updated organic classification of tyrosinase inhibitors on melanin biosynthesis. Current Organic Chemistry, 2015. **19**(1): p. 4-18.
13. Hearing, V.J., *Determination of melanin synthetic pathways.* The Journal of investigative dermatology, 2011. **131**(E1): p. E8.
14. Upadhyay, S., et al., Subcellular compartmentalization and trafficking of the biosynthetic machinery for fungal melanin. Cell reports, 2016. **14**(11): p. 2511-2518.
15. Ismaya, W.T., et al., *Crystallization and preliminary X-ray crystallographic analysis of tyrosinase from the mushroom Agaricus bisporus.* Acta Crystallographica Section F: Structural Biology and Crystallization Communications, 2011. **67**(5): p. 575-578.
16. Ismaya, W.T., et al., Crystal structure of Agaricus bisporus mushroom tyrosinase: identity of the tetramer subunits and interaction with tropolone. Biochemistry, 2011. **50**(24): p. 5477-5486.
17. You, Z., Y.-q. WANG, and Q.-x. HE, *Homology Modeling of Human Tyrosinase.* Journal of Southwest University, 2020. **42**(8): p. 42-48.
18. Peng, Z., et al., Anti-tyrosinase, antioxidant and antibacterial activities of gallic acid-benzylidenehydrazine hybrids and their application in preservation of fresh-cut apples and shrimps. Food chemistry, 2022: p. 132127.
19. Kim, Y.-J. and H. Uyama, Tyrosinase inhibitors from natural and synthetic sources: structure, inhibition mechanism and perspective for the future. Cellular and molecular life sciences CMLS, 2005. **62**(15): p. 1707-1723.
20. Zolghadri, S., et al., *A comprehensive review on tyrosinase inhibitors.* Journal of Enzyme Inhibition and Medicinal Chemistry, 2019. **34**(1): p. 279-309.
21. Kim, Y.-J., et al., New tyrosinase inhibitors,(+)-catechin− aldehyde polycondensates. Biomacromolecules, 2004. **5**(2): p. 474-479.
22. Parvez, S., et al., *Naturally occurring tyrosinase inhibitors: mechanism and applications in skin health, cosmetics and agriculture industries.* Phytotherapy Research: An International Journal Devoted to Pharmacological and Toxicological Evaluation of Natural Product Derivatives, 2007. **21**(9): p. 805-816.
23. Bommareddy, A., et al., Medicinal properties of alpha-santalol, a naturally occurring constituent of sandalwood oil. Natural Product Research, 2019. **33**(4): p. 527-543.
24. Misra, B.B. and S. Dey, Evaluation of in vivo anti-hyperglycemic and antioxidant potentials of α-santalol and sandalwood oil. Phytomedicine, 2013. **20**(5): p. 409-416.
25. Burdock, G.A. and I.G. Carabin, *Safety assessment of sandalwood oil (Santalum album L.).* Food and Chemical Toxicology, 2008. **46**(2): p. 421-432.
26. Dubnicka, M., B. Cromwell, and M. Levine, *Investigation of the Adulteration of Essential Oils by GC-MS.* Current Analytical Chemistry, 2020. **16**(8): p. 965-969.
27. Jain, R. and S. Nair, Sandalwood oil for the chemoprevention of skin cancer: mechanistic insights, anti-inflammatory, and in vivo anticancer potential. Current Pharmacology Reports, 2019. **5**(5): p. 345-358.
28. Haghbeen, K. and E.W. Tan, Direct spectrophotometric assay of monooxygenase and oxidase activities of mushroom tyrosinase in the presence of synthetic and natural substrates. Analytical biochemistry, 2003. **312**(1): p. 23-32.
29. Andrew, S.M., J.A. Titus, and L. Zumstein, *Dialysis and concentration of protein solutions.* Current protocols in toxicology, 2001. **10**(1): p. A. 3H. 1-A. 3H. 5.
30. Wingfield, P., *Protein precipitation using ammonium sulfate.* Current protocols in protein science, 1998. **13**(1): p. A. 3F. 1-A. 3F. 8.
31. Gao, Z., et al., Effect of alkaline extraction pH on structure properties, solubility, and beany flavor of yellow pea protein isolate. Food Research International, 2020. **131**: p. 109045.
32. Pugh, M.E. and E. Schultz, *Assessment of the purification of a protein by ion exchange and gel permeation chromatography.* Biochemistry and Molecular Biology Education, 2002. **30**(3): p. 179-183.
33. Schägger, H., *Tricine–sds-page.* Nature protocols, 2006. **1**(1): p. 16-22.
34. LAEMMLI, U.K., Cleavage of structural proteins during the assembly of the head of bacteriophage T4. nature, 1970. **227**(5259): p. 680-685.
35. Hassan Sajedi, R., et al., *Enzymatic browning, Inhibition, Nitroanilines, Tyrosinase.* Modares Journal of Biotechnology, 2012. **3**(1): p. 67-80.
36. Wilkesman, J. and L. Kurz, *Zymography principles.* Zymography, 2017: p. 3-10.
37. Cui, Y., et al., Inhibition kinetics and molecular simulation of p-substituted cinnamic acid derivatives on tyrosinase. International journal of biological macromolecules, 2017. **95**: p. 1289-1297.
38. Larsson, L.K., Computational and structural characterization of engineered Type-3-copper variants. 2021, Norwegian University of Life Sciences, Ås.
39. Zeng, H.-j., et al., *Investigation on the binding of aloe-emodin with tyrosinase by spectral analysis and molecular docking.* Spectrochimica Acta Part A: Molecular and Biomolecular Spectroscopy, 2019. **211**: p. 79-85.
40. Kim, D., et al., *Flavonoids as mushroom tyrosinase inhibitors: a fluorescence quenching study.* Journal of agricultural and food chemistry, 2006. **54**(3): p. 935-941.
41. Suryawanshi, V.D., et al., Spectroscopic analysis on the binding interaction of biologically active pyrimidine derivative with bovine serum albumin. Journal of Pharmaceutical Analysis, 2016. **6**(1): p. 56-63.
42. Parray, Z.A., et al., Formation of molten globule state in horse heart cytochrome c under physiological conditions: Importance of soft interactions and spectroscopic approach in crowded milieu. International Journal of Biological Macromolecules, 2020. **148**: p. 192-200.

 doi:10.20944/preprints202211.0137.v1

43. Parray, Z.A., et al., Interaction of polyethylene glycol with cytochrome c investigated via in vitro and in silico approaches. Scientific Reports, 2021. **11**(1): p. 6475.
44. Parray, Z.A., et al., Effects of Ethylene Glycol on the Structure and Stability of Myoglobin Using Spectroscopic, Interaction, and In Silico Approaches: Monomer Is Different from Those of Its Polymers. ACS omega, 2020. **5**(23): p. 13840-13850.
45. Mohammad, T., Y. Mathur, and M.I. Hassan, InstaDock: A single-click graphical user interface for molecular docking-based virtual high-throughput screening. Briefings in Bioinformatics, 2021. **22**(4): p. bbaa279.
46. Duong-Ly, K.C. and S.B. Gabelli, Salting out of proteins using ammonium sulfate precipitation, in Methods in enzymology. 2014, Elsevier. p. 85-94.
47. Moringo, N.A., et al., *A mechanistic examination of salting out in protein–polymer membrane interactions.* Proceedings of the National Academy of Sciences, 2019. **116**(46): p. 22938-22945.
48. Hagel, L., *Gel-filtration chromatography.* Current protocols in molecular biology, 1998. **44**(1): p. 10.9. 1-10.9. 2.
49. Lopez-Tejedor, D. and J.M. Palomo, *Efficient purification of a highly active H-subunit of tyrosinase from Agaricus bisporus.* Protein Expression and Purification, 2018. **145**: p. 64-70.
50. Tisserand, R. and R. Young, *Essential oil safety: a guide for health care professionals*. 2013: Elsevier Health Sciences.
51. Pires, D.E., T.L. Blundell, and D.B. Ascher, *pkCSM: predicting small-molecule pharmacokinetic and toxicity properties using graph-based signatures.* Journal of medicinal chemistry, 2015. **58**(9): p. 4066-4072.